THE JOURNAL OF PHYSICAL CHEMISTRY B

Article

pubs.acs.org/JPCB

Binding Preference of Carbon Nanotube Over Proline-Rich Motif Ligand on SH3-Domain: A Comparison with Different Force Fields

Biyun Shi,[†] Guanghong Zuo,[‡,§] Peng Xiu,[∥] and Ruhong Zhou[∥,⊥,*]

[†]Bio-X Lab, Department of Physics, Zhejiang University, Hangzhou 310027, People's Republic of China

[‡]Shanghai Institute of Applied Physics, Chinese Academy of Sciences, P.O. Box 800-204, Shanghai 201800, People's Republic of China

[§]T-Life Research Center, Department of Physics, Fudan University, Shanghai 200433, People's Republic of China

[∥]Soft Matter Research Center and Department of Engineering Mechanics, Zhejiang University, Hangzhou, 310027, People's Republic of China

[⊥]Computational Biology Center, IBM Thomas J. Watson Research Center, Yorktown Heights, New York 10598, United States

Supporting Information

ABSTRACT: With the widespread applications of nanomaterials such as carbon nanotubes, there is a growing concern on the biosafety of these engineered nanoparticles, in particular their interactions with proteins. In molecular simulations of nanoparticle−protein interactions, the choice of empirical parameters (force fields) plays a decisive role, and thus is of great importance and should be examined carefully before wider applications. Here we compare three commonly used force fields, CHARMM, OPLSAA, and AMBER in study of the competitive binding of a single wall carbon nanotube (SWCNT) with a native proline-rich motif (PRM) ligand on its target protein SH3 domain, a ubiquitous protein−protein interaction mediator involved in signaling and regulatory pathways. We find that the SWCNT displays a general preference over the PRM in binding with SH3 domain in all the three force fields examined, although the degree of preference can be somewhat different, with the AMBER force field showing the highest preference. The SWCNT prevents the ligand from reaching its native binding pocket by (i) occupying the binding pocket directly, and (ii) binding with the ligand itself and then being trapped together onto some off-sites. The $\pi-\pi$ stacking interactions between the SWCNT and aromatic residues are found to play a significant role in its binding to the SH3 domain in all the three force fields. Further analyses show that even the SWCNT-ligand binding can also be relatively more stable than the native ligand-protein binding, indicating a serious potential disruption to the protein SH3 function.

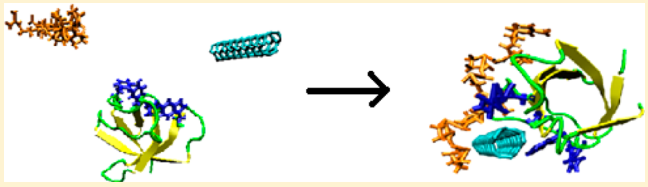

1. INTRODUCTION

A wide variety of interesting and sometimes unexpected properties of nanoparticles, such as carbon nanotubes (CNTs), have been unveiled in recent years,[1,2] resulting in many new applications[3−6] especially in the biomedical field, such as drug delivery,[6,7] cancer diagnoses and therapy.[8−10] However, these nanoparticles, with comparable length scale with biological molecules, are potentially detrimental to human body, because they may block normal biointeraction pathways without being recognized by our immune systems.[11−17] Both experimental and theoretical approaches have shown that the existence of CNTs can significantly affect the biosystems by disrupting the structures or blocking the functions of proteins. For example, obvious local structural distortions were observed after protein streptavidin was bound onto a single-wall carbon nanotube (SWCNT).[18] Karajanagi et al. also observed dramatic changes in both conformation and activity of two enzymes, α-chymotrypsin and soybean peroxidase, upon adsorption onto the SWCNTs.[19] It was found that the conformation of a subdomain of human bovine serum albumin (BSA) could be significantly affected after adsorption onto a SWCNT in molecular dynamics (MD) simulation.[20] Another recent experiment showed that some biological membrane ion channels could be blocked by SWCNTs of certain sizes and shapes.[21] Our MD simulations also showed that the interaction with the nanoparticles might disorder some proteins and disrupt their regular functions.[16,17,22−24] For example, a SWCNT can plug into the hydrophobic cores of WW domains and thereby disrupt their active sites.[24]

Although many efforts have been carried out to understand the biological implications of SWCNTs by computer simulations,[22−29] much less has been done on the basic questions[30] such as how effective these force fields are and how different their results can be, which has prompted our current study on the SWCNT−protein interactions with different force fields. Our recent MD simulations with the AMBER force field have shown that a SWCNT can win the competitive binding over the native proline-rich motif (RPM) ligand on SH3

Received: December 17, 2012
Revised: March 8, 2013
Published: March 11, 2013

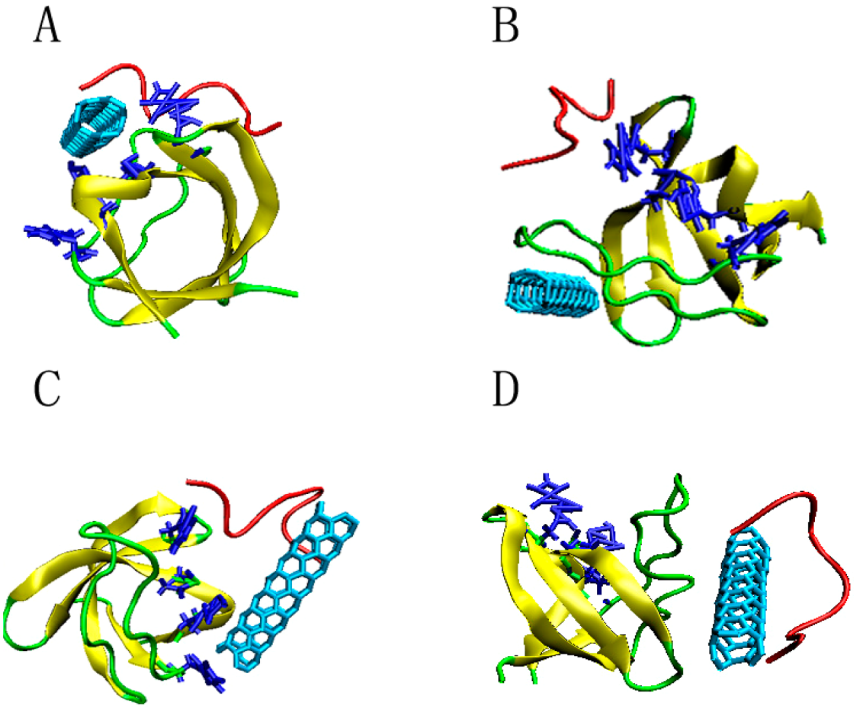

Figure 1. Typical structures of the four different conformational binding patterns. (A) represents SWCNT binding to key residues mainly [pattern (i)]. (B) represents ligand binding to key residues mainly [pattern (ii)]. (C) represents SWCNT and ligand binding to key residues equally [pattern (iii)]. (D) represents that SWCNT and ligand are both away from the key residues [pattern (iv)]. Green and yellow combination represents the SH3 domain on which the blue residues represent the binding pocket. The light blue sticks represent the SWCNT and the red ribbon represents the ligand.

domain, a highly promiscuous protein−protein interaction mediator involved in signaling and regulatory pathways.[23] This observation shows that, in addition to disruption of protein active sites, there is another potential molecular mechanism of CNT's toxicity, i.e., competitive binding with ligands to receptors.[31] However, the results of MD simulations might depend on the force fields used. To test the robustness of this interesting phenomenon and provide further insights into the binding process, we reran the MD simulations with two other commonly used force fields, CHARMM and OPLSAA, and also compared the results with those from AMBER force field. In all three cases, we observed the preferential binding of SWCNT over RPM ligand on SH3 domain, and identified the $\pi-\pi$ stacking interactions between the SWCNT and aromatic residues as important driving force in the binding process, thus demonstrating the robustness of the current observations.

2. METHODS

The current setups of the simulation systems are identical to our previous work[23] except for the force field used, which is switched from AMBER (ffamber03) to CHARMM (charmm27)[32] and OPLSAA,[33] respectively. The three-way ternary binding complex system consists of a SWCNT, a proline-rich motif (RRRVPPRR) ligand, and a c-Crk N-terminal SH3 domain. The SH3 domain is the most abundant protein interaction domain which can identify and bind proline-rich motif ligands.[34−41] The initial structure of the SH3 domain and the ligand were obtained from the Protein Data Bank with PDB code 1CKB.[42] The residue 1 to 8 represents the ligand, and the residue 134 to 190 represents the SH3 domain. The armchair SWCNT (3,3) used in the simulation refers to a tube whose diameter and length are 4.04 Å and 19.54 Å, respectively. The carbon atoms are modeled as uncharged Lennard−Jones particles following previous studies.[23,43,44] The size of the SWCNT is comparable with the ligand.

According to the previous experimental studies, residues F8, W36, P50, and Y53 show a dominant role in binding with the ligand.[35,45] Thus, in order to make the ligand and the SWCNT in an equal competition condition at the first place, they were placed on each side of those four residues, respectively, generating two "mirror-imaging-like" initial conformations. The initial distance between SH3 domain, SWCNT and ligand were both set at 30 Å (far enough to prevent initial interactions). Then, this three-way ternary binding complex was solvated in the TIP3P water,[46] with three Na^+ ions added to neutralize the system. A rhombic dodecahedral periodic box was constructed with the minimum distance between the box boundary and the complex at 12 Å. There were 31 825 and 34 300 atoms in the final systems, respectively (see the previous paper for more details[23]).

Ten MD trajectories were generated for each simulation system. Molecular dynamics simulations have been widely used in the modeling of both biomolecules and nanomaterials to complement experiments,[47−60] which can provide atomic details that are often inaccessible in experiments due to limited resolutions. There were , in total, 40 trajectories, with 20 each for CHARMM and OPLSAA force fields. These newly obtained results were then further compared with the previous results from AMBER force field. Gromacs package 4.5.1[61] was applied for the simulation and software VMD was used to view the trajectories.[62] The long-range electrostatic interactions were treated with the particle-mesh Ewald method (PME) with a grid spacing of 1.2 Å,[63] while the van der Waals interactions were handled with the usual smooth cutoff, with a cutoff

dx.doi.org/10.1021/jp312423y | J. Phys. Chem. B 2013, 117, 3541−3547

distance of 10 Å. The covalent bonds involving H atoms were constrained by the LINCS algorithm with a time step of 2 fs.[64] After energy minimization, the system was equilibrated for 200 ps at a temperature of 298 K and a constant pressure of 1 bar using Berendsen coupling.[65] The production simulation were performed by using the NVT ensemble at T = 298 K.

3. RESULTS AND DISCUSSION

3.1. Direct SWCNT-SH3 Domain Interaction Dominates the 3-Way Ternary Binding. In order to probe the binding competition among the three-way ternary binding complex system (SH3 domain, SWCNT, and ligand), two new force fields (CHARMM and OPLSAA) were applied, in addition to the previously used AMBER force field. Results from all three different force fields are compared, with focus on those new ones from CHARMM and OPLSAA. In general, the trajectories can be classified into four different categories (binding patterns): (i) SWCNT binds to key residues mainly (the SWCNT occupies more key residues than the ligand); (ii) ligand binds to key residues mainly (the ligand occupies more key residues than the SWCNT); (iii) SWCNT and ligand bind to key residues equally (the ligand and the SWCNT occupy two key residues each); and (iv) SWCNT and ligand are both away from key residues (none of them occupy any key residues). Figure 1 displays such typical binding patterns for each category. Table 1 summarizes the occurrence of these different binding patterns in all the trajectories simulated, which clearly shows SWCNT's binding preference over the ligand on the SH3 domain with all the force fields used.

Table 1. Comparison of the Trajectories That Show Different Conformational Binding Patterns with All Three Force Fields

number of the trajectories	SWCNT[a]	ligand[b]	equal[c]	none[d]
CHARMM	7	3	2	8
OPLSAA	7	3	1	9
AMBER	13	1	0	6

[a]SWCNT binds to key residues mainly. [b]Ligand binds to key residues mainly. [c]SWCNT and ligand bind to key residues equally. [d]SWCNT and ligand are both away from key residues.

Both the CHARMM and OPLSAA force fields revealed similar binding patterns. As shown in Table 1, binding pattern (i) (i.e., SWCNT binds to key residues mainly) and (iv) (i.e., SWCNT and ligand are both away from the binding pocket) occurred most frequently in our MD simulations. Only 3 out of 20 trajectories showed some binding preference for pattern (ii) (i.e., the ligand binds to key residues of the SH3 domain mainly). Furthermore, out of these three cases with pattern (ii)-like binding conformations from both force fields, only one trajectory with the CHARMM force field displayed a perfect "matching" structure that resembles that in the PDB structure.[42] Meanwhile, 7 out of 20 trajectories showed binding preference of SWCNT with respect to the SH3 domain (binding pattern (i)) in both CHARMM and OPLSAA cases. It is clear that the SWCNT is more likely to bind with the key residues in the SH3 domain active site, which is consistent with our previous findings with the AMBER force field.[23] However, the degree of preference for the SWCNT is somewhat weaker than that in the AMBER force field. Not only more trajectories showed binding pattern (iv) (both the SWCNT and the ligand were away from the binding pocket) in both CHARMM and OPLSAA, but also less trajectories showed binding pattern (i) (7 in CHARMM and OPLSAA vs 13 in AMBER). In addition, 3 trajectories showed binding pattern (ii) (PRM binding with SH3) in both CHARMM and OPLSAA, while only one showed this same binding pattern (ii) in AMBER. This indicates that the choice of force field does impact the level of the binding preference. Nevertheless, all of the three force fields examined here show consistency in the dominant binding pattern, which is pattern (i), i.e., the SWCNT has a clear binding preference over the ligand when binding onto the SH3 domain.

As mentioned above, there were 7 out of 20 trajectories showing that SWCNT contacts with the key residues in the binding pocket mainly. In most cases of those 7 trajectories, the SWCNT occupied three out of four key residues and bound tightly with the pocket, while the ligand always bound around the SWCNT, indicating the interaction between the ligand and the protein was relatively weak. It sometimes bound to the SWCNT solely with little contact with the protein and sometimes bound to both SWCNT and protein. Even in those trajectories that ligand and SWCNT were both away from the binding pocket, the SWCNT was more likely to bind with the protein. The most possible conformation in those cases was that the SWCNT contacted with the protein directly when the ligand bound on the other side of the SWCNT with few direct contacts with the protein. Meanwhile, it is worth mentioning that in more than 70% of the trajectories, the SWCNT and the ligand bound together in all three force fields. The strong interactions between the SWCNT and the ligand indicate that even if the SWCNT does not occupy the binding pocket, it still shows some capability to prevent the ligand from binding to its native binding pocket. However, the ligand's

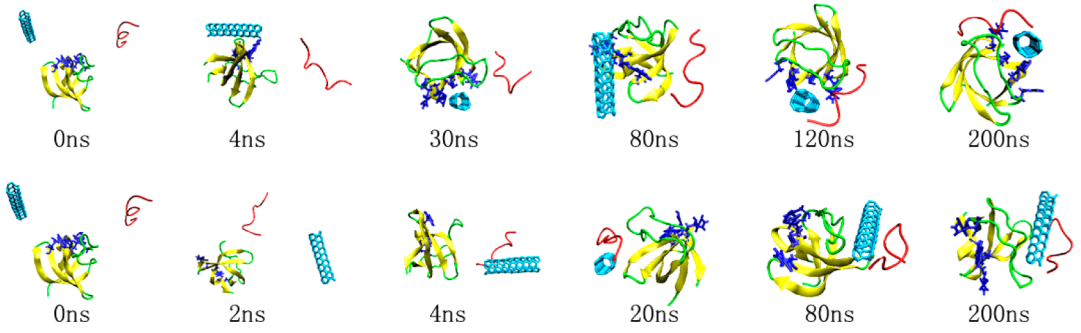

Figure 2. Time evolutions of two typical trajectories which represent two dominant binding patterns, respectively (using the OPLSAA force field as an example). Green and yellow combination represents the SH3 domain on which the blue residues represent the binding pocket. The light blue sticks represent the SWCNT and the red ribbon represents the ligand.

dx.doi.org/10.1021/jp312423y | J. Phys. Chem. B 2013, 117, 3541−3547

preferential binding seems to always happen in the situation that the ligand is not in contact with SWCNT directly and the SWCNT is stuck at some other positions on the protein.

All of the aforementioned results indicate that the SWCNT tends to interact with the key residues of the SH3 domain than the ligand. Furthermore, the strong interaction between the SWCNT and the ligand itself prevents the ligand from approaching its native binding pocket. In one word, the existence of the SWCNT strongly reduces the possibility for the PRM ligand to bind correctly with the SH3 domain, which implies that nanoparticles like carbon nanotubes may be potentially toxic to proteins.

3.2. The Existence of SWCNT Prevents the Ligand from Further Approaching to Its Native Binding Pocket. Figure 2 shows two typical conformational evolutions corresponding to the two dominant binding patterns (i) and (iv) obtained in all three force fields. The exact trajectories used in Figure 2 are obtained by OPLSAA. The upper panel (Figure 2A) represents the trajectories where the SWCNT binds to the key residues mainly [pattern (i)], while the lower panel (Figure 2B) represents the trajectories where both the SWCNT and the ligand are away from the key residues [pattern (iv)].

As shown in Figure 2A, the initial conformation started from a state where the SWCNT and the ligand were well separated and equally away from the SH3 domain. Then, at ~2 ns, the SWCNT approached and contacted on and off with the SH3 domain. From 2 to 32 ns, the ligand finally reached the SH3 domain, but still far from the binding pocket. Meanwhile, the SWCNT adjusted its position on the surface of the protein and finally contacted with key residues W36, P50 and Y53. The binding conformation is quite stable. After that, the ligand also adjusted its position on the SH3 domain and finally contacted with one of the key residues (W36). From this typical trajectory, one can find that (i) the contacts between the SWCNT and the SH3 domain are very stable; (ii) even though the initial binding position of the ligand is not the binding pocket, the ligand can still adjust somewhat to move closer to the binding pocket; (iii) the existence of the SWCNT at the binding pocket prevents the ligand from further approaching to its native binding pocket.

Similarly, for the binding pattern (iv) shown in Figure 2B, the first snapshot displays the initial state of the system. In this case, the ligand showed earlier signs of preference to approach the SH3 domain before the SWCNT (in the first 4 ns). However, before the ligand could reach and bind to the SH3 domain, it bound with the SWCNT first. Then, the SWCNT and ligand binary complex contacted with the SH3 domain together, but not at the binding pocket. At first, they contacted with SH3 domain roughly equally. However, the binding between the ligand and the SH3 domain was not stable. Eventually, direct binding of the ligand to SWCNT, instead of the SH3 domain, served as the ultimate stable conformation, implying the tendency of ligand to bind with SWCNT in this case.

These two dominant binding patterns indicate two possible ways that the existence of the SWCNT can prevent the ligand from binding to its native binding pocket. The first way is that the SWCNT can occupy the binding pocket directly with very stable contacts to the SH3 domain. The second one is that the binding between the SWCNT and the ligand was more stable than the binding between the ligand and the SH3 domain, so that it can prevent the ligand from approaching to its native binding pocket.

3.3. Interplays among the SWCNT, PRM Ligand, and SH3 Domain. In order to obtain a more accurate description about the interactions among the SWCNT, the ligand and the SH3 domain, the contact surface areas of these three binding partners were calculated. The top subfigures of Figure 3 show

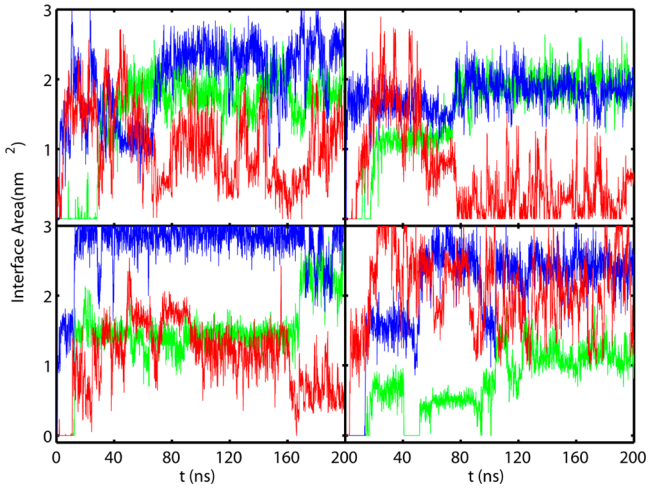

Figure 3. Contact surface areas among SH3 domain, SWCNT and ligand. The top subfigures represent the trajectories from the CHARMM force field, while the bottom subfigures represent the trajectories from the OPLSAA force field. The left and right subfigures correspond to the binding pattern (i) and (iv) in Figure 2, respectively. Blue, red, and green curves represent the contact surface areas between the SWCNT and the SH3 domain, the ligand and the SH3 domain, the SWCNT and the ligand, respectively. Here the contact surface area is defined as half of the difference between the solvent accessible surface area of the complex of the two objects and the sum of the solvent accessible surface areas of the two objects separately.

the two typical trajectories from the CHARMM force field, while the bottom subfigures of Figure 3 show the trajectories from the OPLSAA force field. The left and right subfigures correspond to the binding pattern (i) and (iv) in Figure 2, respectively. Although not all of the trajectories behaved exactly the same as in these two representative ones, they did represent the typical conformational evolutions. The top left subfigure showed that at the beginning (within 10 ns), the SWCNT and the ligand approached the SH3 domain and stuck to the surface at different positions. Then, from 10 to 40 ns, the SWCNT and the ligand adjusted their positions on the SH3 domain and contacted with each other. The system was relatively stable after 80 ns, and the final conformation indicated that the SWCNT contacted with the SH3 domain mainly while the ligand contacted with both the SWCNT and the SH3 domain partially [representing binding pattern (i)]. Obviously, the contacts between the SWCNT and SH3 domain (or the ligand) were relatively stable, while the contacts between the ligand and the SH3 domain were less stable or more flexible. Similarly, the top right subfigure represented another conformational binding pattern (iv) that the SWCNT and the ligand were both away from the key residues. Even though the ligand approached the SH3 domain at the beginning, the contact surface area between them dropped sharply when the ligand started its contact with the SWCNT. Even when both the SWCNT and the ligand were away from the binding pocket, the SWCNT still showed some preference to contact with the SH3 domain, while the ligand preferred to contact with the SWCNT rather than the

dx.doi.org/10.1021/jp312423y | J. Phys. Chem. B 2013, 117, 3541−3547

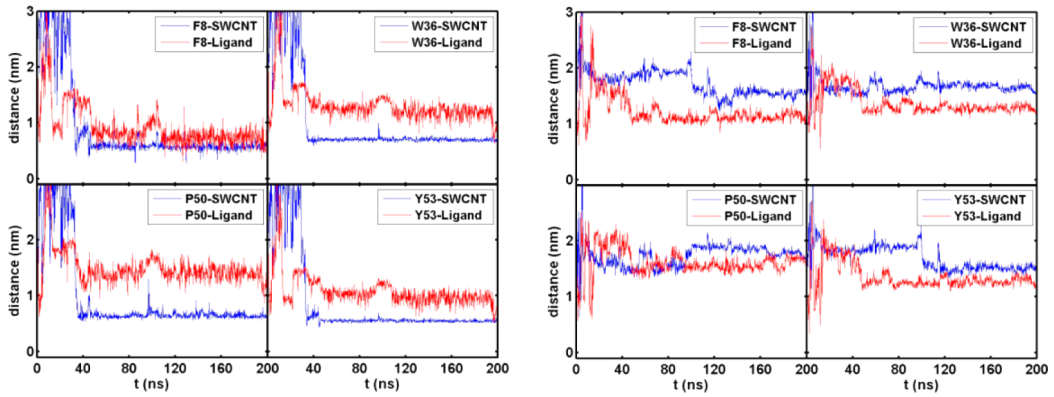

Figure 4. Minimum distance of the SWCTN (blue) and the ligand (red) with the key residues (F8, W36, P50 and Y53) of the SH3 domain. The left subfigures represent the trajectories that the SWCNT occupies the binding pocket [binding pattern (i)]. The right subfigures represent the trajectories that both the SWCNT and the ligand are away from the binding pocket [binding pattern (iv)].

SH3 domain. The contact surface areas from the OPLSAA force field showed similar behavior as those from the CHARMM force field, therefore, we conclude that the binding between the SWCNT and the SH3 domain was quite stable in both CHARMM and OPLSAA, while the ligand was more likely to bind with the SWCNT. This is consistent with findings from our previous study[23] using the AMBER force field, indicating the high binding preference between the SWCTN and protein does not change with different force fields.

To further characterize the binding among the SWCNT, the ligand, and the SH3 domain, the distances of the SWCNT and the ligand from the key residues were also calculated. Figure 4 shows the distances of two representative trajectories obtained from the CHARMM force field.

In the left subfigures of Figure 4, the distances between the key residues F8, P50, and Y53 and the SWCNT were much shorter than the ligand, which implied that the SWCNT contacted with these residues and occupied the binding pocket. Meanwhile, the distances between the residues W36, SWCNT and the ligand were similar, indicating that although the SWCNT occupied the binding pocket, the ligand still had some capability to move closer to the key residues. In the right subfigures, the distances of SWCNT and the ligand from the key residues were all more than 1 nm, indicating that they were both away from the binding pocket. The results from the OPLSAA and AMBER force fields were similar to those displayed for the CHARMM force field. Note that F8, Y53, and W36 all belong to aromatic residues, indicating that the $\pi-\pi$ stacking interactions between the SWCNT and aromatic residues play an important role in the binding process (some may question the accuracy of classical fixed-charge force fields, and our previous study[30] has demonstrated that the popular classical force fields can appropriately reproduce the strength of $\pi-\pi$ interactions between protein and CNT). Therefore, our simulations show that the $\pi-\pi$ stacking interactions play a dominant role in the binding between the SWCNT and the SH3 domain, and the underlying main driving force does not change with different force fields.

Meanwhile, to further characterize the differences among different force fields, we have calculated the binding free energy landscapes for OPLSAA and CHARMM force fields as well, using the same reaction coordinates as in the previous AMBER case. The results are shown in Supporting Information, Figure S1. In the OPLSAA force field, the SWCNT displays ~0.2 kcal/mol stronger binding free energy than the ligand (−5.49 vs −5.28 kcal/mol), while in the CHARMM case, the ligand is ~0.3 kcal/mol lower than the SWCNT (−5.22 vs −5.54 kcal/mol). Even though the SWCNT does not always show a stronger binding energy (which depends on the reaction coordinates used to some degree), these binding free energy values are very comparable. It should be noted that it does not need SWCNT to have an extraordinarily high binding affinity to interfere the protein−ligand binding (thus signal transduction), comparable bindings would suffice to inhibit or interrupt the protein function. In addition, the detailed landscape shapes do differ from force field to force field, indicating there are differences in the atomic-detailed interactions despite the overall similarity.

4. CONCLUSIONS

The binding competition between an SWCNT and a proline-rich motif (PRM) ligand to the target protein SH3 domain was studied with MD simulations using three commonly used force fields. The SWCNT displays a general binding preference over the ligand onto the SH3 domain in all three force fields, but the degree of preference is somewhat different, with the AMBER force field showing the highest preference while CHARMM and OPLSAA sharing a similar preference. This indicates that the choice of force field does not change the binding preference qualitatively, but does impact the level of binding preference somewhat. There are two ways in which the SWCNT prevents the ligand from approaching to its native binding pocket on the SH3 domain. The first way is that the SWCNT occupies the binding pocket itself through its stronger binding with the SH3 domain. The second one is that the SWCNT binds with the ligand first forming a binary complex, and then stick together onto some off-sites on the SH3-domain. This also indicates that the ligand binds tighter with the SWCNT than the SH3 domain. The detailed analysis of the contact surface areas and the distances of the SWCNT (ligand) from the key residues further confirm these conclusions. Essentially, the interactions between the SWCNT and the SH3 domain, the SWCNT and the ligand, are relatively more stable than the interaction between the ligand the SH3 domain. The dominant SWCNT-SH3 domain binding implies that the $\pi-\pi$ stacking interactions between the SWCNT and aromatic residues play an important role in the binding process.

dx.doi.org/10.1021/jp312423y | J. Phys. Chem. B 2013, 117, 3541−3547

■ ASSOCIATED CONTENT

Supporting Information

Binding free energy landscapes of the SWCNT and the ligand with the SH3 domain using OPLSAA and CHARMM force fields. This material is available free of charge via the Internet at http://pubs.acs.org.

■ AUTHOR INFORMATION

Corresponding Author

*Tel: (914) 945-3591; fax: (845) 489-9512; e-mail: ruhongz@us.ibm.com (R.Z.).

Notes

The authors declare no competing financial interest.

■ ACKNOWLEDGMENTS

Thanks for the helpful discussions with Zaixing Yang, Seung-gu Kang, and Bo Zhou. This research is partly supported by National Natural Science Foundation of China (Grant No. NSFC11104308 and 11204269), Zhejiang Provincial Natural Science Foundation of China (Grant No. LY12A04007), Fundamental Research Funds for the Central Universities, and KYLIN-I supercomputer in Institute for Fusion Theory and Simulation, Zhejiang University. R.Z. acknowledges the support from the IBM Blue Gene Science Program.

■ REFERENCES

(1) Guldi, D. M.; Rahman, A.; Sgobba, V.; Ehli, C. *Chem. Soc. Rev.* **2006**, *35*, 471−487.
(2) Goldberger, J.; Fan, R.; Yang, P. D. *Acc. Chem. Res.* **2006**, *39*, 239−248.
(3) Rutherglen, C.; Jain, D.; Burke, P. *Nat. Nanotechnol.* **2009**, *4*, 811−819.
(4) Wilson, N. R.; Macpherson, J. V. *Nat. Nanotechnol.* **2009**, *4*, 483−491.
(5) Krauss, T. D. *Nat. Nanotechnol.* **2009**, *4*, 85−86.
(6) Kam, N. W. S.; Jessop, T. C.; Wender, P. A.; Dai, H. J. *J. Am. Chem. Soc.* **2004**, *126*, 6850−6851.
(7) Kam, N. W. S.; Liu, Z.; Dai, H. J. *J. Am. Chem. Soc.* **2005**, *127*, 12492−12493.
(8) Liu, B.; Li, X.; Li, B.; Xu, B.; Zhao, Y. *Nano Lett.* **2009**, *9*, 1386−1394.
(9) De la Zerda, A.; Zavaleta, C.; Keren, S.; Vaithilingam, S.; Bodapati, S.; Liu, Z.; Levi, J.; Smith, B. R.; Ma, T. J.; Oralkan, O.; et al. *Nat. Nanotechnol.* **2008**, *3*, 557−562.
(10) Liu, Y.; Wang, H. *Nat. Nanotechnol.* **2007**, *2*, 20−21.
(11) Zhao, Y.; Xing, G.; Chai, Z. *Nat. Nanotechnol.* **2008**, *3*, 191−192.
(12) Jia, G.; Wang, H. F.; Yan, L.; Wang, X.; Pei, R. J.; Yan, T.; Zhao, Y. L.; Guo, X. B. *Environ. Sci. Technol.* **2005**, *39*, 1378−1383.
(13) Poland, C. A.; Duffin, R.; Kinloch, I.; Maynard, A.; Wallace, W. A. H.; Seaton, A.; Stone, V.; Brown, S.; MacNee, W.; Donaldson, K. *Nat. Nanotechnol.* **2008**, *3*, 423−428.
(14) Ali-Boucetta, H.; Al-Jamal, K. T.; Kostarelos, K. *Methods Mol. Biol.* **2011**, *726*, 299−312.
(15) Lam, C.-w.; James, J. T.; McCluskey, R.; Arepalli, S.; Hunter, R. L. *Crit. Rev. Toxicol.* **2006**, *36*, 189−217.
(16) Kang, S. G.; Zhou, G.; Yang, P.; Liu, Y.; Sun, B.; Huynh, T.; Meng, H.; Zhao, L.; Xing, G.; Chen, C.; et al. *Proc. Natl. Acad. Sci. U. S. A.* **2012**, *109*, 15431−15436.
(17) Ge, C.; Du, J.; Zhao, L.; Wang, L.; Liu, Y.; Li, D.; Yang, Y.; Zhou, R.; Zhao, Y.; Chai, Z.; et al. *Proc. Natl. Acad. Sci. U. S. A.* **2011**, *108*, 16968−16973.
(18) Zhong, J.; Song, L.; Meng, J.; Gao, B.; Chu, W.; Xu, H.; Luo, Y.; Guo, J.; Marcelli, A.; Xie, S.; et al. *Carbon* **2009**, *47*, 967−973.
(19) Karajanagi, S. S.; Vertegel, A. A.; Kane, R. S.; Dordick, J. S. *Langmuir* **2004**, *20*, 11594−11599.
(20) Goldberg-Oppenheimer, P.; Regev, O. *Small* **2007**, *3*, 1894−1899.
(21) Park, K. H. *J. Biol. Chem.* **2003**, *278*, 50212−50216.
(22) Zuo, G.; Huang, Q.; Wei, G.; Zhou, R.; Fang, H. *ACS Nano* **2010**, *4*, 7508−7514.
(23) Zuo, G.; Gu, W.; Fang, H.; Zhou, R. *J. Phys. Chem. C.* **2011**, *115*, 12322−12328.
(24) Zuo, G.; Zhou, X.; Huang, Q.; Fang, H.; Zhou, R. *J. Phys. Chem. C.* **2011**, *115*, 23323−23328.
(25) Agashe, M.; Raut, V.; Stuart, S. J.; Latour, R. A. *Langmuir* **2004**, *21*, 1103−1117.
(26) Raffaini, G.; Ganazzoli, F. *J. Phys. Chem. B.* **2004**, *108*, 13850−13854.
(27) Cormack, A. N.; Lewis, R. J.; Goldstein, A. H. *J. Phys. Chem. B.* **2004**, *108*, 20408−20418.
(28) Shen, J.-W.; Wu, T.; Wang, Q.; Pan, H.-H. *Biomaterials* **2008**, *29*, 513−532.
(29) Shen, J.-W.; Wu, T.; Wang, Q.; Kang, Y. *Biomaterials* **2008**, *29*, 3847−3855.
(30) Yang, Z.; Wang, Z.; Tian, X.; Xiu, P.; Zhou, R. *J. Chem. Phys.* **2012**, *136*, 025103.
(31) Zuo, G.; Kang, S. G.; Xiu, P.; Zhao, Y.; Zhou, R. *Small* **2012**, in press.
(32) MacKerell, A. D.; Bashford, D.; Bellott; Dunbrack, R. L.; Evanseck, J. D.; Field, M. J.; Fischer, S.; Gao, J.; Guo, H.; Ha, S.; et al. *J. Phys. Chem. B.* **1998**, *102*, 3586−3616.
(33) Jorgensen, W. L.; Maxwell, D. S.; Tirado-Rives, J. *J. Am. Chem. Soc.* **1996**, *118*, 11225−11236.
(34) Venter, J. C.; Adams, M. D.; Myers, E. W.; Li, P. W.; Mural, R. J.; Sutton, G. G.; Smith, H. O.; Yandell, M.; Evans, C. A.; Holt, R. A.; et al. *Science* **2001**, *291*, 1304−1351.
(35) Ball, L. J.; Kuhne, R.; Schneider-Mergener, J.; Oschkinat, H. *Angew. Chem.* **2005**, *44*, 2852−2869.
(36) Bucciantini, M.; Giannoni, E.; Chiti, F.; Baroni, F.; Formigli, L.; Zurdo, J.; Taddei, N.; Ramponi, G.; Dobson, C. M.; Stefani, M. *Nature* **2002**, *416*, 507−511.
(37) Gorina, S.; Pavletich, N. P. *Science* **1996**, *274*, 1001−1005.
(38) Macias, M. J.; Wiesner, S.; Sudol, M. *FEBS Lett.* **2002**, *513*, 30−37.
(39) Zarrinpar, A.; Bhattacharyya, R. P.; Lim, W. A. *Science's STKE* **2003**, *2003*, RE8.
(40) Li, X.; Chen, Y.; Liu, Y.; Gao, J.; Gao, F.; Bartlam, M.; Wu, J. Y.; Rao, Z. *J. Biol. Chem.* **2006**, *281*, 28430−28437.
(41) Kobashigawa, Y.; Sakai, M.; Naito, M.; Yokochi, M.; Kumeta, H.; Makino, Y.; Ogura, K.; Tanaka, S.; Inagaki, F. *Nat. Struct. Mol. Biol.* **2007**, *14*, 503−510.
(42) Wu, X.; Knudsen, B.; Feller, S. M.; Zheng, J.; Sali, A.; Cowburn, D.; Hanafusa, H.; Kuriyan, J. *Structure* **1995**, *3*, 215−226.
(43) Hummer, G.; Rasaiah, J. C.; Noworyta, J. P. *Nature* **2001**, *414*, 188−190.
(44) Xiu, P.; Tu, Y.; Tian, X.; Fang, H.; Zhou, R. *Nanoscale* **2012**, *4*, 652−658.
(45) Nguyen, J. T.; Turck, C. W.; Cohen, F. E.; Zuckermann, R. N.; Lim, W. A. *Science* **1998**, *282*, 2088−2092.
(46) Jorgensen, W. L.; Chandrasekhar, J.; Madura, J. D.; Impey, R. W.; Klein, M. L. *J. Chem. Phys.* **1983**, *79*, 926−935.
(47) Duan, Y.; Kollman, P. A. *Science* **1998**, *282*, 740−744.
(48) Levy, Y.; Wolynes, P. G.; Onuchic, J. N. *Proc. Natl. Acad. Sci. U. S. A.* **2004**, *101*, 511−516.
(49) Snow, C. D.; Nguyen, H.; Pande, V. S.; Gruebele, M. *Nature* **2002**, *420*, 102−106.
(50) Zhou, R.; Huang, X.; Margulis, C. J.; Berne, B. J. *Science* **2004**, *305*, 1605−1609.
(51) Liu, P.; Huang, X.; Zhou, R.; Berne, B. J. *Nature* **2005**, *437*, 159−162.
(52) Zuo, G.; Hu, J.; Fang, H. *Phys. Rev. E.* **2009**, *79*, 031925.
(53) Mayor, U.; Guydosh, N. R.; Johnson, C. M.; Grossmann, J. G.; Sato, S.; Jas, G. S.; Freund, S. M. V.; Alonso, D. O. V.; Daggett, V.; Fersht, A. R. *Nature* **2003**, *421*, 863−867.

(54) Garcia, A. E.; Paschek, D. *J. Am. Chem. Soc.* **2007**, *130*, 815−817.
(55) Miyashita, N.; Straub, J. E.; Thirumalai, D. *J. Am. Chem. Soc.* **2009**, *131*, 17843−17852.
(56) Zheng, L.; Chen, M.; Yang, W. *Proc. Natl. Acad. Sci. U. S. A.* **2008**, *105*, 20227−20232.
(57) van der Vaart, A.; Karplus, M. *J. Chem. Phys.* **2005**, *122*, 114903.
(58) Eleftheriou, M.; Germain, R. S.; Royyuru, A. K.; Zhou, R. *J. Am. Chem. Soc.* **2006**, *128*, 13388−13395.
(59) Li, X.; Li, J.; Eleftheriou, M.; Zhou, R. *J. Am. Chem. Soc.* **2006**, *128*, 12439−12447.
(60) Tu, Y.; Xiu, P.; Wan, R.; Hu, J.; Zhou, R.; Fang, H. *Proc. Natl. Acad. Sci. U. S. A.* **2009**, *106*, 18120−18124.
(61) Hess, B.; Kutzner, C.; van der Spoel, D.; Lindahl, E. *J. Chem. Theory Comput.* **2008**, *4*, 435−447.
(62) Humphrey, W.; Dalke, A.; Schulten, K. *J. Mol. Graph.* **1996**, *14*, 33−38.
(63) Essmann, U.; Perera, L.; Berkowitz, M. L.; Darden, T.; Lee, H.; Pedersen, L. G. *J. Chem. Phys.* **1995**, *103*, 8577−8593.
(64) Hess, B.; Bekker, H.; Berendsen, H. J. C.; Fraaije, J. G. E. M. *J. Comput. Chem.* **1997**, *18*, 1463−1472.
(65) Berendsen, H. J. C.; Postma, J. P. M.; van Gunsteren, W. F.; DiNola, A.; Haak, J. R. *J. Chem. Phys.* **1984**, *81*, 3684−3690.